Relative Roles of Large-Scale Orography and Land Surface Processes in the Global Hydroclimate. Part II: Impacts on Hydroclimate over Eurasia

KAZUYUKI SAITO

Frontier Research Center for Global Change, Japan Agency for Marine-Earth Science and Technology, Yokohama, Kanagawa, Japan

TETSUZO YASUNARI

Frontier Research Center for Global Change, Japan Agency for Marine-Earth Science and Technology, Yokohama, Kanagawa, and Nagoya University, Nagoya, Aichi, Japan

KUMIKO TAKATA

Frontier Research Center for Global Change, Japan Agency for Marine-Earth Science and Technology, Yokohama, Kanagawa, Japan

(Manuscript received 12 May 2005, in final form 5 January 2006)

ABSTRACT

A series of simplistic simulations from an AGCM coupled to a simple land surface scheme and water vapor tracers was performed to explore the relative roles of basic factors in land surface conditions, with regard to the seasonal evolution of the hydroclimate over Eurasia. Large-scale orography in Asia and vegetation (further decomposed to soil and vegetation skin) were evaluated, with orography represented in the model by surface altitude, soil represented by water-holding capacity, and vegetation skin represented by surface albedo and roughness.

The percentage of global annual precipitation over land (occupying 25.6% of the total surface) was 14.8%, 15.0%, and 21.7% for the mountainless "bare rock" (i.e., vegetationless) surface, and the bare-rock and vegetated surface, respectively. The result for evaporation was 8.9%, 9.0%, and 16.2%, respectively, showing higher sensitivity to the land surface changes than precipitation. The orography and vegetation (i.e., soil and vegetation skin) showed different impacts on Eurasian hydroclimate on the seasonal and regional scales. Thermodynamical forcings to the atmosphere increased over the continent with the inclusion of both. Large-scale orography in Asia exerted east–west contrast in the surface energy exchange in summer in eastern Eurasia. An increase in extratropical winter precipitation with mountains was also noticed because of the atmospheric vapor transport changes. Impact of soil and vegetation skin was clearly found in the warm season in the extratropics; soil impacts extratropical summer precipitation due to enhanced recycling of water and the resultant increased water supply.

1. Introduction

Water is fundamental to the planetary ecoclimate system. Understanding the variability and availability of water over land is a significant issue for human societies. Variability in the hydroclimate over land is closely and directly linked to land surface conditions and processes. Although the role of the ocean, the largest reservoir of water on earth, cannot be exaggerated, the land surface conditions determine an important aspect of water and energy exchanges with the atmosphere and affect the amount and variability of water flow and storage, especially over land. Monsoon activity is a prominent example of a land role in the global hydroclimate. Recent analyses of the temporal variability of remotely sensed oceanic water vapor show large annual variations only near continental coastal areas that coincide with the major monsoon regions (Chen 2004); variability is smaller over the open ocean. Such enhanced variability near land implies how the presence and conditions of land may be important in the continental hydroclimate. The present-day land surface conditions comprise of several individual pro-

Corresponding author address: Kazuyuki Saito, FRCGC/JAMSTEC, 3173-25 Showa-Machi, Kanazawa-Ku, Yokohama City, Kanagawa 236-0001, Japan.
E-mail: ksaito@jamstec.go.jp

cesses or conditions that have been developed through time. Our fundamental question is which of the individual conditions that comprises the present land surface may be relatively more important to the current continental hydroclimate.

Beginning in the late nineteenth century, pedologists, or soil scientists, recognized that topography, vegetation (organism), soil, and climate mutually interact to constitute a system near the earth's surface (Jenny 1941; Buol et al. 1997). Soil has formed through physical and chemical processes such as weathering, and through biological processes for which vegetation has played an important role. In other words, soil layer is a product of vegetation activity in collaboration with climate, and must be treated explicitly when the basic effect of vegetation is concerned. In turn, soil has provided a vital base for vegetation and other organisms. In Asia, the uplift of the Tibetan Plateau must have played a decisive role in shaping the continental to hemispheric atmospheric circulation patterns and the hydroclimate of the continent. Grounded on the above speculations, we choose *large-scale orography* and *vegetation* as key conditions. The latter may be conceptually decomposed further into *soil* and *surface vegetation*. "Bare rock"—that is, a soilless, vegetationless surface—is termed a *nonvegetated* land surface. Our attempt reflects some important stages or components, of relatively long time scale, in the evolution of the earth's surface from the paleoclimatic past (bare rock without the Tibetan Plateau) to the present continental surface.

There have been a number of model studies on land surface effects on climate. They, however, tend to have focused on one or a few specific processes or conditions, separately. Examples include studies on the effects of orography or land–sea geometry (Hahn and Manabe 1975; Broccoli and Manabe 1992; Kutzbach et al. 1993; Dirmeyer 1998), albedo (Charney et al. 1975, 1977; Dirmeyer and Shukla 1996), vegetation (Sato et al. 1989; Xue et al. 2004), and soil wetness (Delworth and Manabe 1988, 1989; Milly and Dunne 1994; Douville et al. 2001). An investigation, attempting to evaluate the relative importance of these land surface conditions on the hydroclimate in one outline, has not been completed.

To this purpose, an atmospheric general circulation model (AGCM) coupled to a simple land surface scheme was used under an idealistic experiment design. In this study, we aimed at delineating a simplistic picture of the basic mechanism evolved over millions of years, with the same configuration. Our simple scheme, however, includes the basic vegetation processes of relatively long time scale, such as surface albedo and roughness length, and indirectly considers the effect of transpiration. The conditions of large-scale topography, soil, and surface vegetation are parameterized in the model by surface altitude, by water-holding capacity or field capacity; and by vegetation skin (surface albedo and roughness), respectively. Note that "surface vegetation" in this study, therefore, refers only to the vegetation skin since the model does not include subgrid-scale, biospheric parameterizations. Similarly, (total) vegetation or vegetated surface is a reference only to the "soil layer with vegetation skin" in this study. Relevant details of the important land surface processes in the simple scheme are described in the next section. A thorough description of the scheme is found in the first part of this study (Yasunari et al. 2006, hereafter Part I). We set the horizontal resolution at T42 (almost equivalent to 2.8° gridding in latitude and longitude) for computational efficiency, so that we can derive monthly climatology from 50-yr realization, and pentad climatology from 25-yr simulation.

Part I of this study evaluated the relative roles of land surface processes on monsoon activity and the related large-scale atmospheric circulation in the Tropics. Here, in Part II, the climatology and seasonality of the continental hydroclimate is discussed, with a special focus on extratropical eastern Eurasia. Section 2 briefly describes the model and the experiment design. Sections 3 through 6 show the results of the analysis. Discussions and concluding remarks are given in section 7.

2. Model and experiment design

Part I contains detailed descriptions of the model and experiment design. Only a brief outline therefore is presented here. The model, the Center for Climate System Research/National Institute for Environmental Studies/Frontier Research Center for Global Change (CCSR/NIES/FRCGC) AGCM, is a three-dimensional hydrostatic primitive equation model with spherical and sigma coordinates. The model is run at T42 horizontal resolution with 20 vertical levels up to about 10 hPa in the lower stratosphere. Ocean surface conditions (sea surface temperatures and sea ice concentration) are prescribed using a monthly climatology derived from 1979–89 observations that were prepared and used for the Atmospheric Model Intercomparison Project (Gates 1992).

Soil moisture amount is an important factor in controlling the amount of water and energy fluxes from the land to the atmosphere. Soil water content is prognostically determined in the scheme in one layer through the balance of precipitation, evapotranspiration, snowmelt, and runoff in the simple hydrology scheme (Num-

aguti 1999). The water-holding capacity (saturation soil water storage) of the 1-m soil layer is defined by field capacity (FC). Default value of the FC is 20 cm, considering soil porosity, gravity drainage, and available depth for vegetation.

Surface albedo affects the rate of incoming solar radiation absorbed at the surface and thus the amount of available energy at the surface. Roughness is used in diagnostic estimation of the aerodynamic resistance. In the simple land scheme we used, surface albedo and roughness length (Z_0) are specified in accordance with the prescribed vegetation type, although change in amount of leaf or canopy is not explicitly accounted for since no vegetation physiology is included in the scheme.

Vertical turbulent fluxes at the surface are estimated by bulk formulas. Aerodynamic resistance is diagnostically determined, and stomatal resistance is set to the daytime or nighttime value according to the local solar angle if vegetation is present, and thus the transpiration is included in a simple way. The evaporation efficiency is then estimated from soil wetness, aerodynamic resistance, and stomatal resistance.

Four simulations with different land surface conditions comprised the study: a bare-rock surface with no orography in Asia (NMR), the bare-rock surface (MR), a desert condition (MS), and a vegetated condition (MVS). The bare-rock surface mimics nonvegetated state. The vegetation type was specified to desert where albedo and roughness length (Z_0) were 0.30 and 0.02 m, respectively, and field capacity was set to 1 cm. The default topography was used except for the NMR run, in which it is set to zero east of 30°E in the Asian region including the Arabian Peninsula to simulate the absence of the large-scale orography (cf. Fig. 2 in Part I). In the MS run, FC was set to the default value of 20 cm to represent the soil layer. The MS condition is a virtual complementary setting to bridge the bare-rock and vegetated conditions. The MVS run used the default vegetation type, FC, and surface altitude. Thus, albedo and Z_0 were specified according to the vegetation type at each grid point. Table 1 in Part I summarizes the experiment design.

For each of the four simulations, the model was run for 50 yr after a 5-yr spinup. Monthly climatology for simulated variables was calculated for the last 40 simulation years; pentad climatology was derived from the final 25 yr.

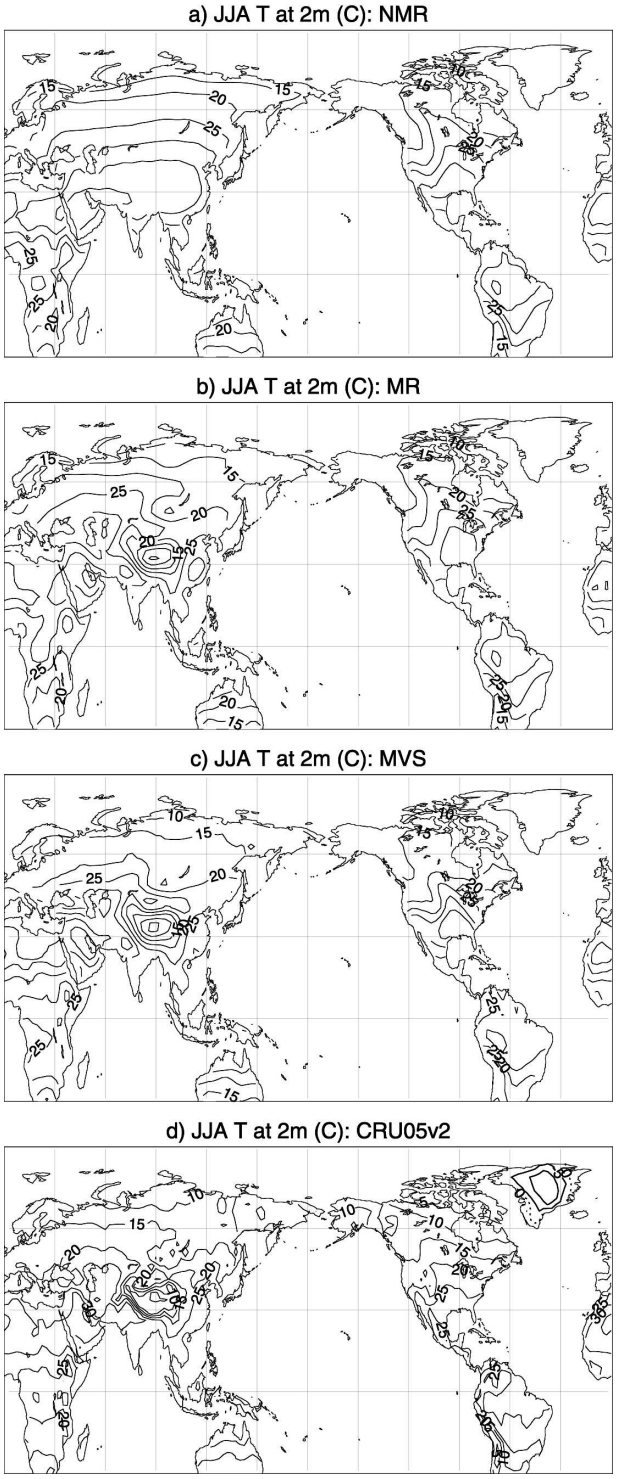

FIG. 1. (a) Surface air temperature at 2 m (T2m) in summer (JJA) for (a) NMR, (b) MR, (c) MVS, and (d) observation. Contour interval is 5°C.

3. Near-surface energy balance

Figure 1 shows the summer [June–August (JJA)] climatology for near-surface air temperatures for the (a)–

(c) simulations and (d) observations. Boreal seasons are used in this paper unless otherwise stated. The observed climatology was calculated from the Climatic Research Unit (CRU) time series (TS) 2.0 dataset provided at the University of East Anglia, United Kingdom (Mitchell and James 2005), for the same period used to derive the SST climatology. Comparison of regional precipitation with observed values is discussed in Part I (cf. Fig. 4 in Part I).

Figure 2 shows the impact of the land surface conditions on summer near-surface air temperature. Positive values are contoured with thick lines and filled with dark shades, while negative values are contoured thin and are shaded lightly. We discuss in this section only summer climatology for it is the season in which the impact of vegetation is acknowledged in the broadest regions. Seasonal change will be discussed in the next section. Presence of the orography (i.e., MR minus NMR) decreases local surface temperatures following the atmospheric lapse rate (Fig. 2a). Figures 2b and 2c show apparently offsetting impacts of soil and vegetation skin on temperature, being emphasized in the extratropics. Sensible heat decreases (and consequently surface air temperature decreases) due to an increase of soil moisture and resultant latent heat flux in the MS run, while net radiation increases (leading to increased surface air temperature) due to vegetation albedo in the MVS run. The model's climatology of near-surface air temperature is simulated reasonably well in the Tropics and subtropics, but tends to overestimate north of 40°N by several degrees in both seasons (Fig. 1d). The reason for the warm bias is not clear. Lack of subgrid biospherical parameterization (e.g., canopy layer and root-to-leaf transpiration mechanism) may account for the bias to some degree (Sato et al. 1989). Another possible factor is the insufficient implementation of processes related to soil freezing and permafrost (Luo et al. 2003; Viterbo et al. 1999), for the used land surface scheme is not enough to resolve the soil-freezing processes. For other meteorological variables, spatial patterns and magnitudes in the MVS climatology were reasonably in agreement with the observation to similar extent (not shown), and we considered them sufficient for our purpose.

The land surface conditions give a large impact on surface energy balance, and consequently the thermodynamical forcing at the land surface to the atmosphere. Figure 3 illustrates the changes in the total amount of surface available energy, defined here as a sum of surface sensible and latent heat flux to the atmosphere. The surface energy balance in the model is expressed by the following equation at the infinitely thin skin of the surface:

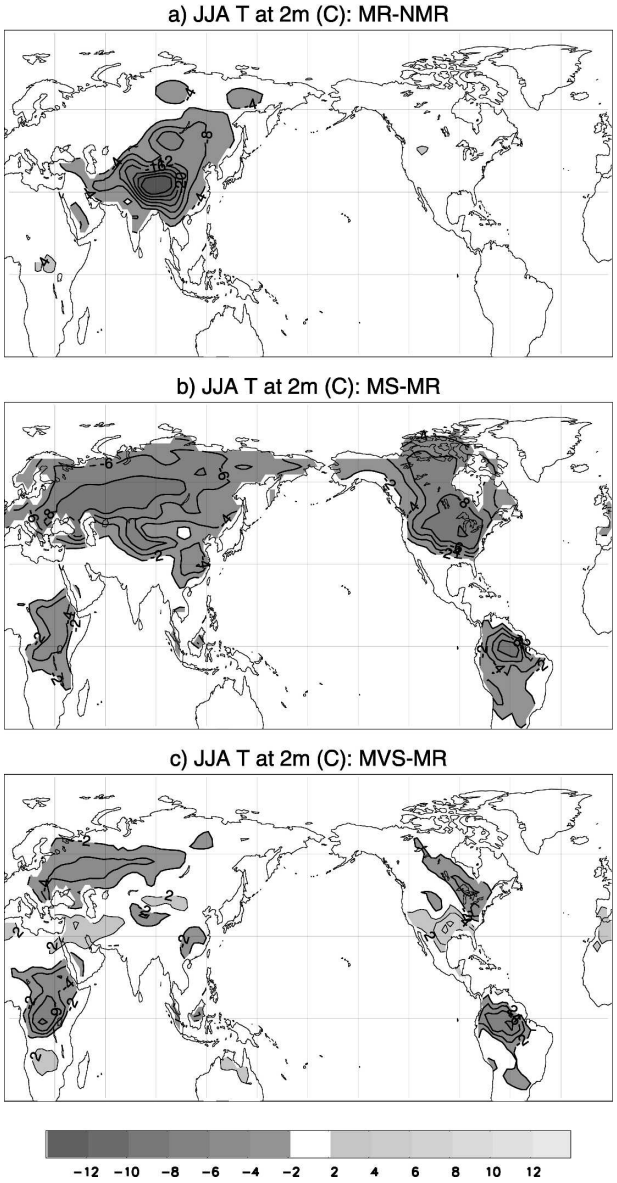

FIG. 2. Difference of JJA T2m between (a) MR and NMR runs, (b) MS and MR runs, and (c) MVS and MR runs. Contour interval is 4°C. Positive values are shaded lightly and negative values heavily.

$$S^{\downarrow} + S^{\uparrow} + L^{\downarrow} + L^{\uparrow} = H + \lambda E + G,$$

where $S^{\downarrow}(S^{\uparrow})$ denotes downward (upward) shortwave radiation, $L^{\downarrow}(L^{\uparrow})$ denotes downward (upward) longwave radiation, and H and λE denote sensible and latent heat flux to/from the atmosphere, respectively. Here G is ground heat conduction and latent heat used in snowmelt. The left-hand side (lhs) of the equation is the net radiation absorbed at the surface and equals the total available energy at surface for heat fluxes. The amount of ground heat conduction and snowmelt latent

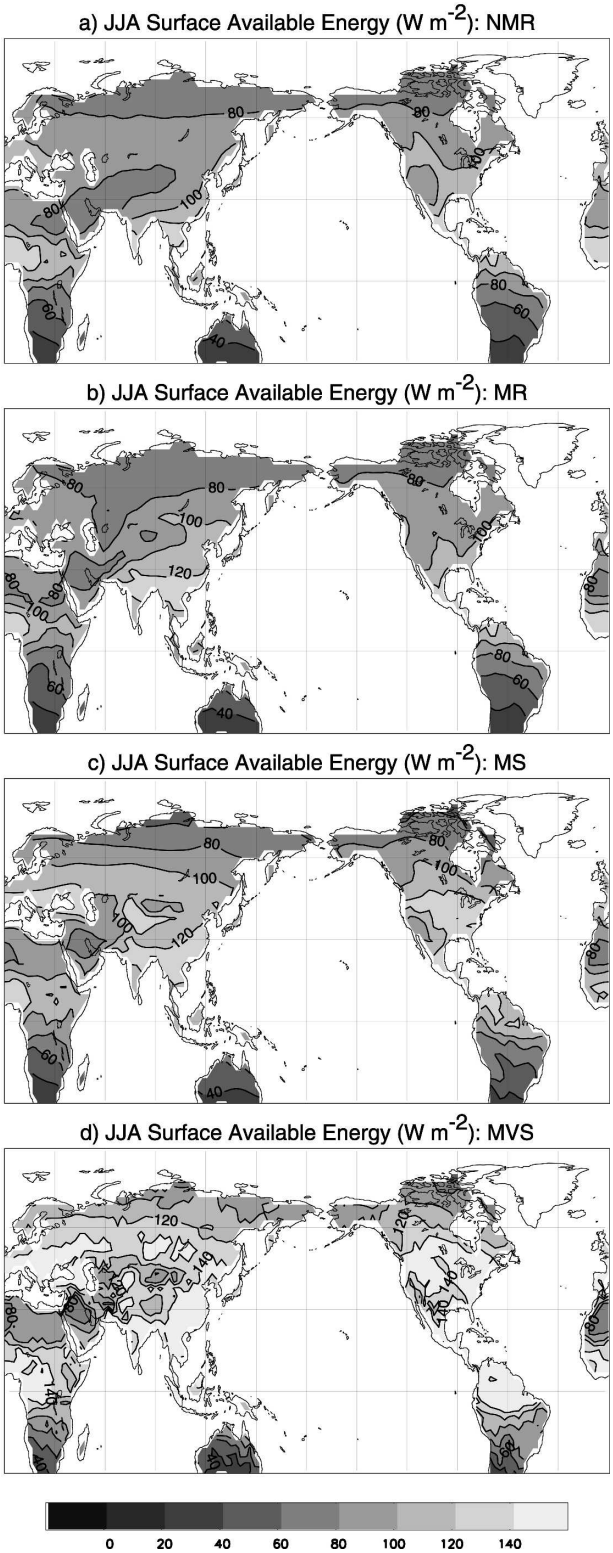

FIG. 3. Surface available energy for (a) NMR, (b) MR, (c) MS, and (d) MVS run. Contour interval is 20 W m^{-2}.

heat is usually small, especially in summer, compared to the first two terms on the right-hand side (rhs) of the equation, and therefore we refer to the sum of sensible and latent heat flux as the "surface available energy" in the following analysis. The distribution of the surface available energy over land was substantially similar to that of the sum of two column-integrated atmospheric heating terms, apparent heat source Q_1, and apparent moisture source $-Q_2$ since the column-integrated atmospheric radiative heating was minor compared to the sum of the two terms. Surface available energy in the MVS run was in good agreement with the observed in eastern Eurasia (Yanai and Li 1994).

The fraction of sensible heat flux F_H in the partition of the surface available energy is defined by the following equation:

$$F_H = H/(H + \lambda E),$$

and is shown in Fig. 4. The surface available energy decreases in general monotonically from the equator to the pole, reflecting the hemispheric difference in the solar radiation. The sensible seat fraction also has a meridional distribution in Eurasia, but modified by an east–west contrast regarding the distance from the ocean (Figs. 3a, 4a). The continental area of the subtropical high, from North Africa through the Arabian Peninsula to the southern central Asia, shows a relatively small amount of surface available energy for its latitude, and high fraction of sensible heat. In contrast, the eastern areas close to the ocean have relatively large surface available energy and lower fraction of sensible heat, likely resulting from moisture advection from the oceans associated with monsoon activity. Mountains and vegetation affect the total amount and partition of the surface available energy at different places with different magnitudes.

The large-scale orography increased the amount of the local surface available energy by about 20 W m^{-2} (Fig. 3b) and decreased the sensible heat fraction to the area (Fig. 4b), thereby creating an east–west contrast. This increase in heating of the lower atmosphere from surface is consistent with the argument on the Tibetan Plateau's role on the Asian summer monsoon from the observational side (e.g., He et al. 1987; Yanai et al. 1992) and from the numerical side (e.g., Hahn and Manabe 1975; Dirmeyer 1998). Increased moisture availability due to changes in the atmospheric moisture transport may also account for the change (cf. Fig. 5 in Part I). In contrast, surface available energy is smaller and the sensible heat fraction is larger in the western part of central Asia where the surface is drier due to precipitation decrease (cf. Figs. 3a,b in Part I). Broccoli

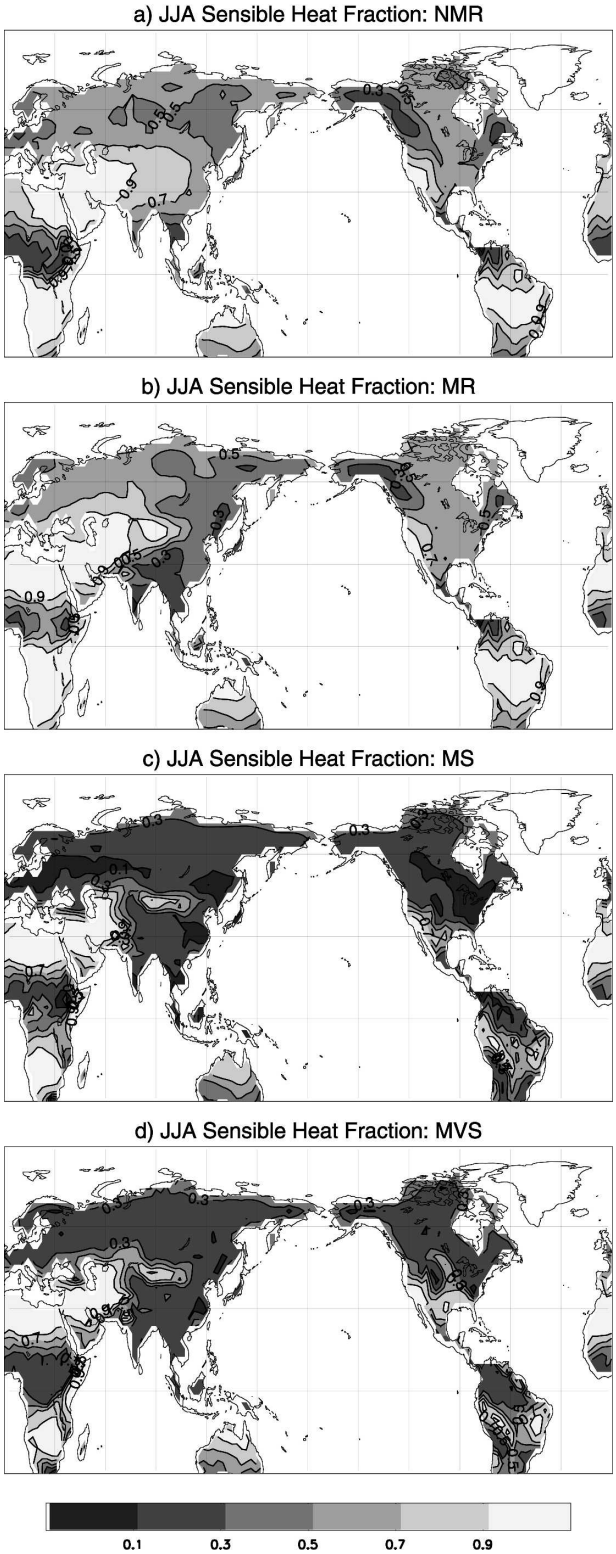

FIG. 4. As in Fig. 3, but for sensible heat fraction.

and Manabe (1992) examined effects of orography with and without soil moisture feedback in the midlatitude continent. Our result for the MR–NMR (Figs. 3a,b) is consistent with their results (their Figs. 15, 16) in that the presence of orography leads to an arid condition in central Asia. However, the result of the difference to MS or MVS is compared: it shows less arid conditions in the region (Fig. 4 in Part I), as also seen in surface available balance in Fig. 3. This may result from different soil moisture capacity; their NM run (no mountains with interactive soil moisture) has the FC value of 15 cm compared to 1 cm for our NMR run, and may indicate the amount of moisture capacity is more relevant than interactivity of soil moisture. Asian topography had small but discernible impact on the amount of surface available energy in remote regions too, for example, near the Rocky Mountains (topography outside Asia remains unchanged between the NMR and MR simulations), and central to West Africa. For the latter, the influence of the Tibetan Plateau on atmospheric circulation and African climate has been discussed in several studies (e.g., Rodwell and Hoskins 1996) and in Part I.

When vegetation is present (in MS and MVS), the surface available energy increases and sensible heat fraction decreases in large areas in the continent (Figs. 3c,d and 4c,d). Zonally uniform distribution of surface available energy is emphasized by the soil layer, with larger meridional gradient than for the NMR case (Fig. 3c). The sensible heat fraction decreases to one-third or smaller except the subtropical high regions, likely due to increased availability of soil moisture to evaporation in the MS run (Fig. 4c), and surface air temperature decreases (Fig. 2b). The vegetation skin (albedo and roughness), specified according to the vegetation type at each grid point, changes the local-scale distribution of the available energy at the surface, although it adds only a minor impact on the sensible heat fraction (Fig. 4d). Patchiness of the available energy reflects the distribution of vegetation types and their albedo (cf. Fig. 2a in Part I). This additional decrease in albedo by vegetation skin works to increase the net radiation, and surface available energy increases, leading to surface air temperature increase. Thereby, both sensible and latent heat increase, keeping the ratio of partition almost the same, since the soil layer is present to provide moisture (Figs. 3c,d and 4c,d). The results and argument by Charney et al. (1977) of positive feedback between albedo, atmosphere (convection), and precipitation, especially in the midlatitude semiarid areas, is in line with the difference shown between MVS and MS runs as far as surface temperature and energetics are concerned (their Tables 4.3–4).

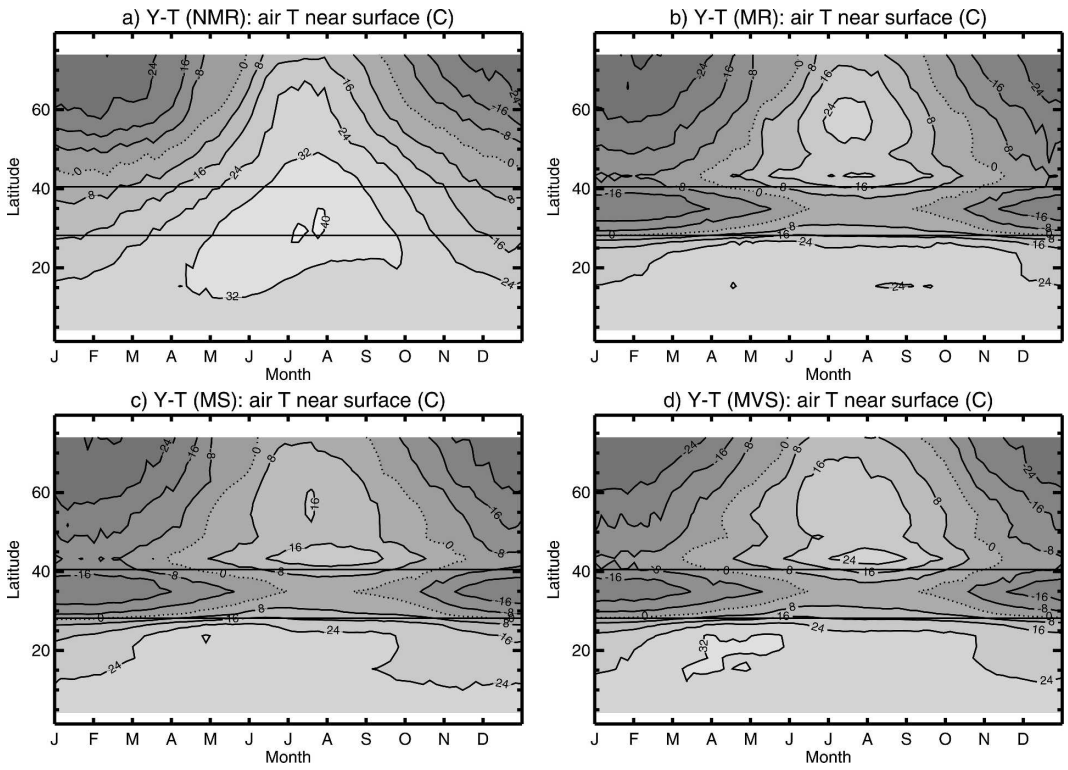

FIG. 5. (a) Time–latitude cross section of air temperature near surface averaged over the area between 70° and 100°E for the (a) NMR, (b) MR, (c) MS, and (d) MVS runs. Contour interval is 8°C. Two horizontal black solid lines denote the region of high orography, including the Tibetan Plateau.

4. Seasonal transitions over Asian land regions

Changes in land surface conditions led not only to different seasonal climatology, as demonstrated in Part I and in the previous section, but also to different seasonal evolution of the continental hydroclimate. Latitude–time characteristics of continental hydroclimate under different land surface conditions are compared in a meridional strip between 70° and 100°E, using pentad climatology. This geographical area includes, from south to north, India, western Indochina, Tibet, the Tarim Basin, and the Siberian Plain and Plateau. Various climate sections of Eurasia are included, from moist Tropics to arid arctic areas and from coastal regions to the continental interior.

a. Near-surface air temperature

Figure 5 shows latitude–time sections of near-surface air temperature (T_s) averaged over the strip defined above. The area between the two horizontal solid black lines denotes the latitude band of high orography that includes the Tibetan Plateau. Mean altitude in this region exceeds 2000 m.

For all the seasons, local surface air temperature decreases following the atmospheric lapse rate if the Tibetan Plateau is absent (Fig. 5a; cf. Fig. 2a). The latitudinal distribution of T_s is either monomodal (summer) or monotonic (other seasons) without the orography. The highest temperature would exceed 40°C in summer around 30°N; a descending motion would prevail and no topographically forced convective clouds appear to give a shade. The northern continent is less changed with or without the orography, but its amplitude of the seasonal change is suppressed with vegetation. In the tropical region, the seasonal amplitude changes with orography, but less impact is found with soil and vegetation skin.

b. Precipitation

Figure 6 shows the similar plots for precipitation. A northward jump in the precipitation center, associated with the onset of the south Asian monsoon, is found in the all the simulations, although the duration, intensity, and geographical extent of the jump are different. For the NMR run, it is rather a mild migration rather than a jump. It reiterates the results of the previous studies (e.g., Hahn and Manabe 1975; Dirmeyer 1998; Abe et al. 2003) that the Tibetan Plateau is attributable to the progress of the Asian monsoon precipitation as it is

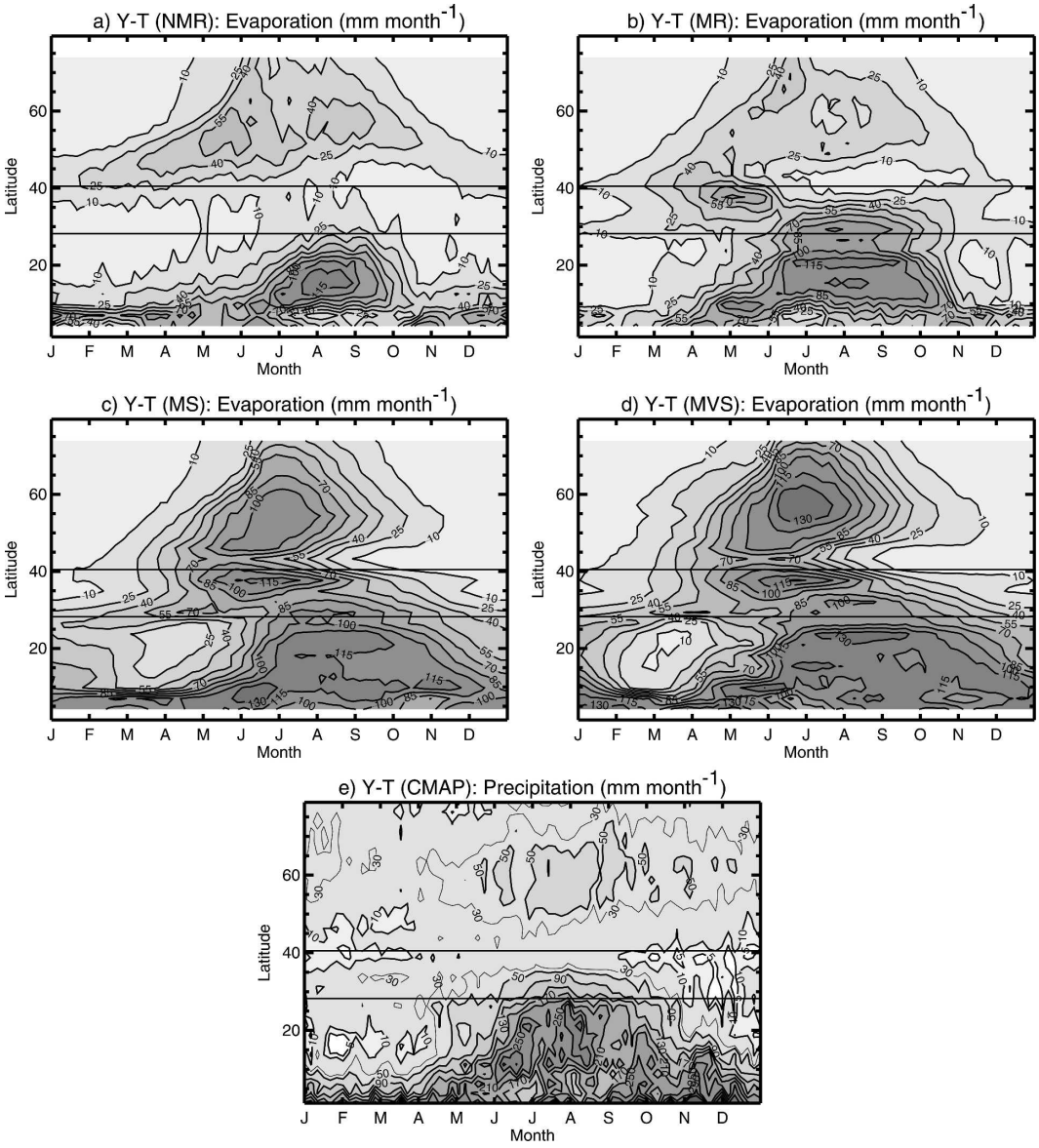

FIG. 6. (a)–(d) As in Fig. 5, but for precipitation (mm month^{-1}). Contours are drawn at 5, 10, 50, and 90 mm month^{-1}. (e) As in (a) but from CMAP.

observed in the present days. Vegetation adds a small modification to make the onset of the summer monsoon earlier, the timing of the precipitation shift, and the rainy season long.

In the extratropics, rainfall will be very small if the surface has no soil layer to store moisture and has a small seasonal cycle (Figs. 6a,b), for the Eurasian continent is a global moisture source in summer and a sink in winter (Fig. 2 in Numaguti 1999). With large-scale orography, a zonal band between 40° and 60°N will be wetter except for midsummer, resulting in even smaller seasonal change due to changed atmospheric circulation (Fig. 6b). This contrast of drying north and moistening south is consistent with the previous studies noted above. The summer monsoon season is the most extensive period, but other seasons shows a similar tendency with smaller amplitude. With vegetation, the extratropical continent has more precipitation during the warm season, leading to a longer seasonal cycle with a larger amplitude. The presence of soil is largely responsible for the change in summer precipitation (almost doubled in the simulation). It has long been acknowledged that water-storage capacity of the surface (i.e., soil layer) and consequent evaporation have a large influence on continental precipitation. It is more evident in semiarid areas and the extratropics than in the

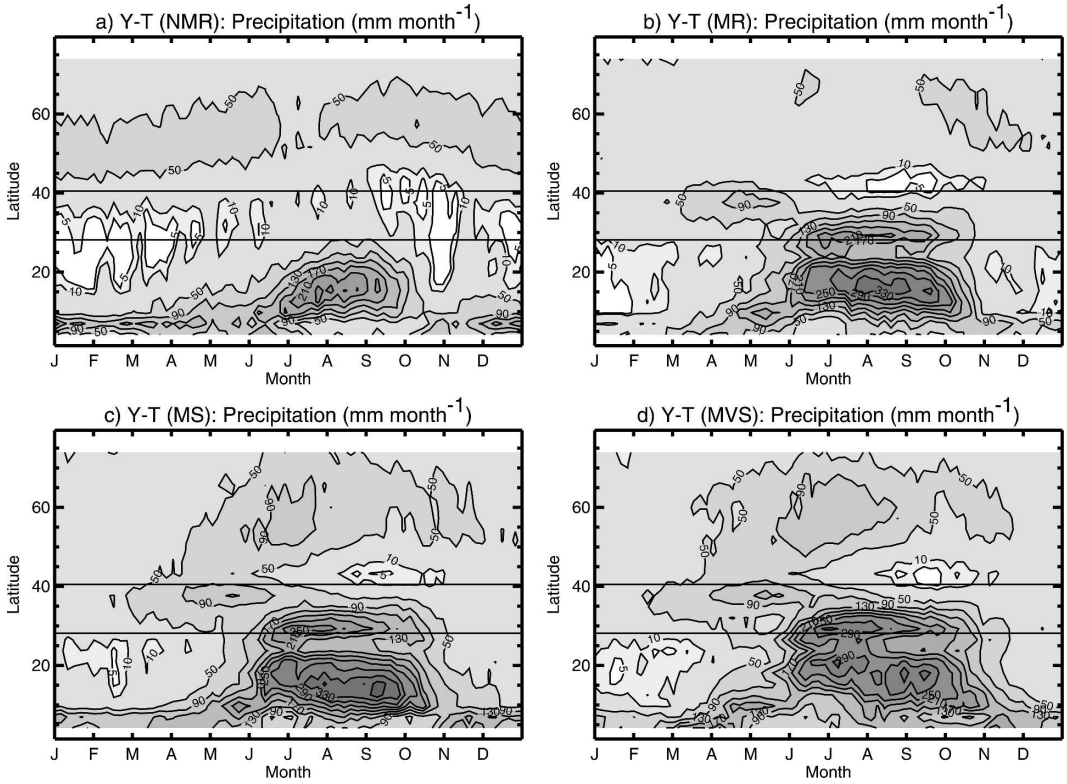

FIG. 7. As in Fig. 5 but for evaporation (mm month^{-1}). Contour interval is 15 mm month^{-1}, beginning from 10 mm month^{-1}.

Tropics (Fig. 1 in Shukla and Mintz 1982; Fig. 2 in Milly and Dunne 1994). The vegetation skin further accelerates the start of rainy season by up to two months.

The simulated amount of precipitation in the extratropical continents for the MS and MVS run is higher than the observed present-day values taken from the Climate Prediction Center (CPC) Merged Analysis of Precipitation (CMAP; Xie and Arkin 1997) (Fig. 6e; cf. Figs. 4 and 11 in Part I). The reasons of this overestimation are not fully clear yet, but at least two factors appear to be attributable, to some extent: one is the warm bias of air temperatures from the surface to the upper troposphere, and the other is the overestimation tendency of evaporation in the simple surface scheme, as will be discussed later. With a warm bias and an excess of evaporation, the air column tends to have more precipitable water, possibly bringing more precipitation to the column. Parameterization related to cloud formation and precipitation processes may also be responsible for the bias. However, it is out of our scope.

c. *Evaporation*

The amount of moisture flux (evaporation), or latent heat flux, is directly related to the water-holding capacity of the land surface. Changes in latent heat have partly been discussed in section 3. Seasonal change in evaporation in the extratropical continent is synchronous with the annual solar cycle regardless of the surface conditions, as shown in Fig. 7. In the extratropical continent, uplift of mountains exerts only a small decrease, corresponding to a drier condition as noted before (Figs. 6a,b). With vegetation, the evaporation rate increases drastically. Despite the increase in the amplitude, the phase does not change with the surface conditions. This is a characteristic of continental evaporation cycle at high latitudes that it is largely phase locked with the available energy cycle. Evaporation enhancement occurs during the warm rainy season in high latitudes, likely due to the short time scale of water vapor residence in the atmosphere and to a positive feedback between evaporation and precipitation. Increased evaporation enhances additional vapor for precipitation, and more precipitation further increases local evaporation. Reduced albedo and the resultant increase in the surface available energy, and the increased storage of soil moisture, augment the high-latitude evaporation by about 100 mm month^{-1} in the MVS simulation. Additional analysis on precipitation and evaporation changes by vapor tracking will be

given in section 6. The result of increased evaporation with the soil layer appears to be reasonable, in comparison with previous studies (e.g., Milly and Dunne 1994). In fact, the difference between the MR and MS (or MVS) runs for evaporation and precipitation are consistent with the result of Milly and Dunne (1994; cf. their Figs. 4 and 6). The absolute value, however, may be overestimated because of the overestimation tendency in the simple hydrology scheme employed in this study, when compared with advanced biosphere–hydrology schemes, such as Simple Biosphere Model (SiB; Sato et al. 1989) variants or other recent schemes (Henderson-Sellers et al. 2003). Sato et al. (1989) demonstrated the difference may exceed 25 W m^{-2} in the large areas of the continents during summer, except for the arid regions.

To the contrary, the evaporation rate in the Tropics is more closely related to the precipitation cycle, or water availability, because the surface available energy is usually abundant in the region. Uplift of the Tibetan surface increases the monsoon-related precipitation, which consequently increases evaporation from spring to autumn over the Tibetan Plateau and in the Tropics (Figs. 7a,b). With vegetation, evaporation further increases during the dry season (November to next March), likely because of the prolonged rainy season and stored water for simultaneous or delayed evaporation.

5. Hydrometeorology north of 40°N over continental Eurasia

a. Low-level cloud (stratocumulus)

Low-level clouds (defined in the model as the percentage of cloud cover below 680 hPa) can trace synoptic-scale disturbances and frontal activities at mid- and high latitudes (Fig. 8). Continental low-level cloudiness in MVS in Fig. 8d was overestimated at mid-latitude winter and underestimated from mid- to high latitudes in other seasons when compared to a climatology derived from International Satellite Cloud Climatology (ISCCP) (Fig. 8e). Nonetheless, the seasonal change is qualitatively reproduced, sufficient to discuss the relative impacts of land surface processes on the seasonal cycle of synoptic-scale disturbances in the region.

Asian orography exerts a small impact on low-level cloud cover. It delays the northern migration in summer, by a month or shorter, at 70°N or higher. The cloud cover decreases in the band between 50° and 70°N for the other seasons in the mountain case (Fig. 8b).

In MS run, the low-level cloud cover is more extensive at high latitudes in the warm season, compared to MVS run. Charney et al. (1977) showed that a decrease in net radiation at the surface and a resulting decrease in transfer of surface energy, due to increased albedo, lead to a decrease in total cloud cover in semiarid area (their Tables 4.2–4). In our MS and MVS runs, summer cloud cover decreases with increased surface albedo in the subtropical semiarid regions in good agreement with Charney's results (not shown), but it increases in the extratropics, showing a different result from theirs (Figs. 8c,d). The lower-tropospheric air from 50° to 70°N in MS run is found to contain less specific humidity and the dry-bulb temperature is noticed to be much colder compared to the MVS run, resulting in higher relative humidity but lower equivalent potential temperature. The meridional equivalent potential temperature gradient is larger in the lower troposphere and, speculatively, more favorable for baroclinic instability in the MS run, and organized upward motion is evident at the latitudes (not shown). The large cloud cover in the MS run, however, does not bring precipitation to the surface, only keeping temperatures cooler at the surface and in the lower troposphere by reducing the solar radiation. Cloud cover is smaller in MVS (Fig. 8d), except only at midsummer in the higher latitude north of 75°N. It may be argued that at latitudes 50°–70°N, baroclinic instability is less favored and upward motion is weak, likely attributed to smaller meridional temperature gradients for the most areas. The low-level cloud distribution reproduced in each simulation was consistent with the ambient conditions regarding the baroclinic instability and upward motions. However, the cloud representation of the AGCM has a systematic bias as noted before, which implies some insufficiencies in the cloud parameterization or large-scale condensation. The warm bias of surface air temperatures, discussed in section 3, may also be related to the cloud parameterization, to some extent. Further investigation will be needed to examine the robustness of the above results and discussion. In early spring (March to April), the northward shift of the synoptic activities starts earlier and at higher latitude in the MVS run, in accordance with earlier snowmelt in the region as discussed shortly.

b. Snow hydrology in Siberia

In this section we look at impacts on the seasonal cycle of the snow hydrology in a region between 50° and 80°N and 80° and 140°E, defined as Siberia. Figure 9 shows the monthly change, starting in August, of total precipitation, solid precipitation (snowfall), snowmelt, and accumulated snow-water equivalent (snow depth).

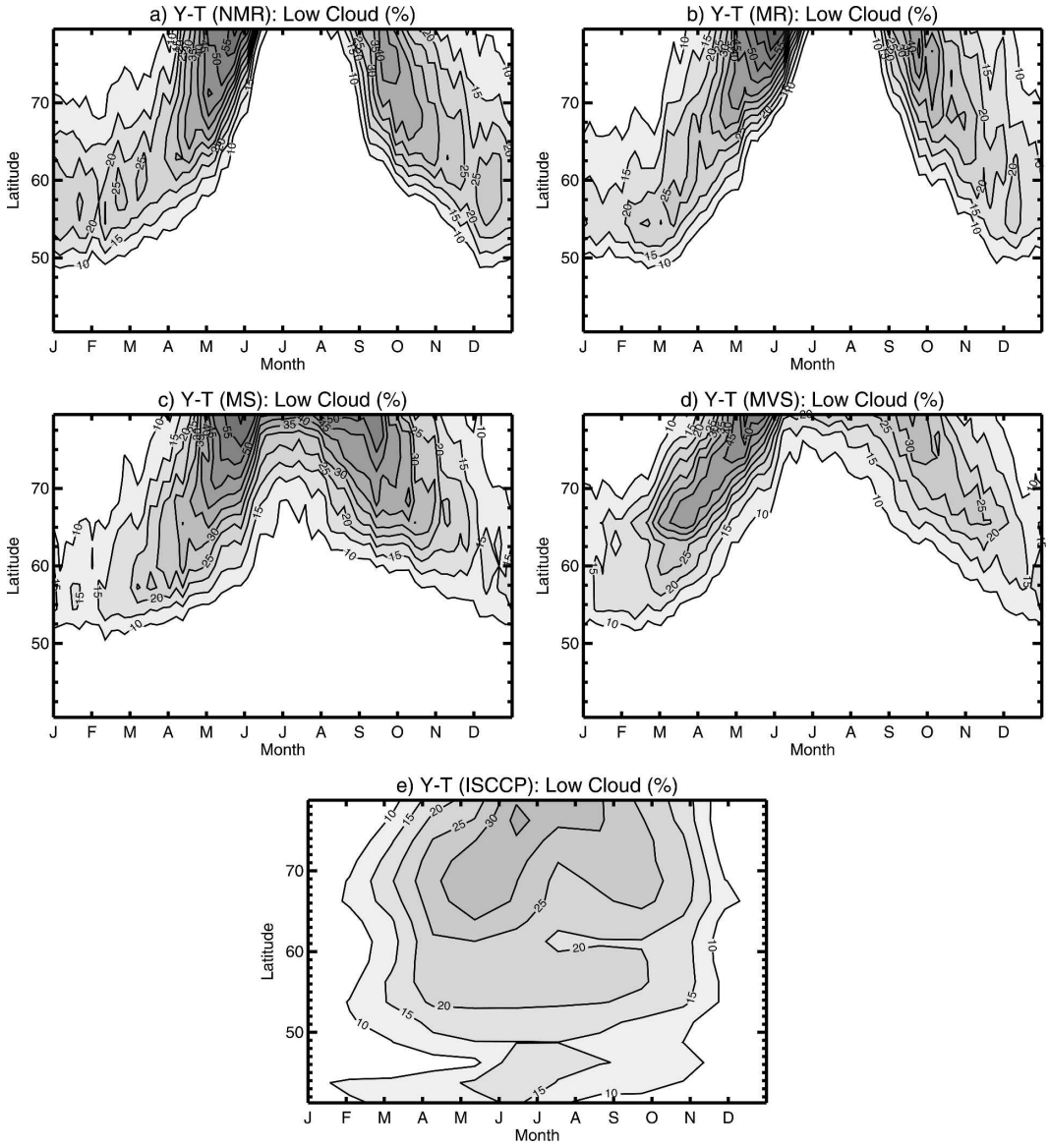

FIG. 8. (a)–(d) As in Fig. 5, but for percentage of low-level cloud cover (surface to 680 hPa) between 40° and 80°N. Contour interval is 5, beginning at 10%. (e) As in (a) but for monthly low cloud cover from ISCCP.

The presence of large-scale Asian orography significantly altered the total and seasonal distribution of precipitation over extratropical Eurasia. Without mountains the seasonal cycle of precipitation has only a small amplitude, with higher winter precipitation (all in solid form). The maximum snow accumulation is deeper by a quarter than with the mountains (MR). In spring, snowfall ends early and snowmelt is faster, leading to a shorter snow accumulation season in the NMR case.

The impact of vegetation is apparent on snow hydrology in the extratropical continent, and the influence of vegetation skin is dominating especially from late winter to spring. Snow accumulation is lower in the MVS run than in the MS or MR runs because temperatures are warmer in late summer/early autumn, resulting in later snow accumulation (Fig. 9d). Snowmelt starts earlier in MVS, reflecting warmer lower-tropospheric air temperatures with vegetation (cf. Figs. 5b–d). This is parallel to the early peak both in snow-water equivalent and in snowmelt by two pentads (Figs. 9c,d). After snowmelt starts, precipitation (liquid or solid) in the MVS run becomes higher than in the other two (MS and MR) runs. This enhanced precipitation is consistent with the faster northward displacement of synoptic-scale disturbances shown in Fig. 8d. The impact of soil is largely seen in summer, as precipitation amount

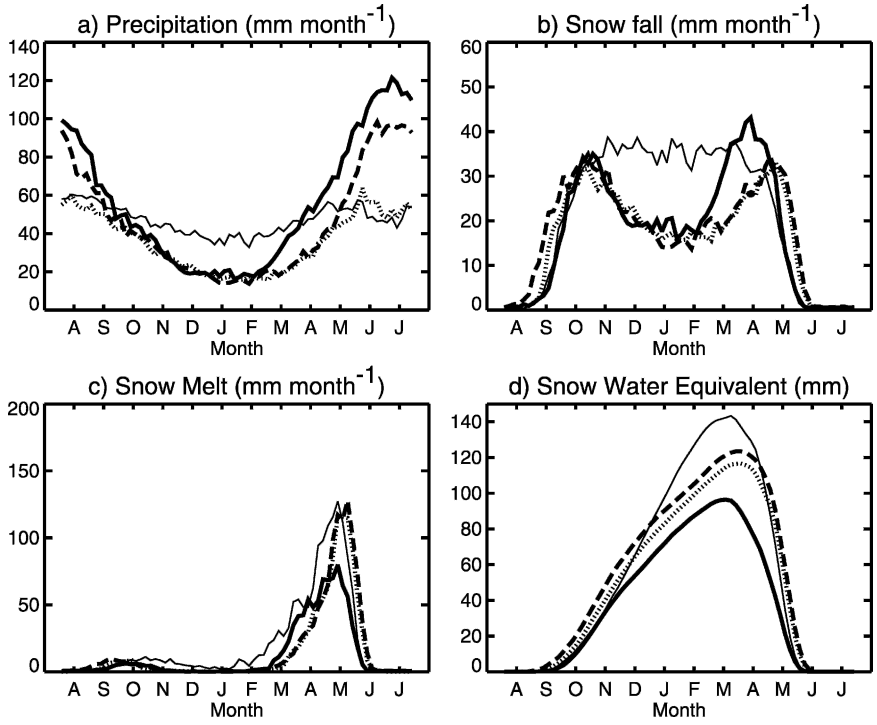

FIG. 9. (a) Monthly total precipitation (mm month^{-1}) for NMR (thin solid), MR (dotted), MS (dashed), and MVS (solid). (b) As in (a) but for snowfall (mm month^{-1}). (c) As in (a) but for snowmelt (mm month^{-1}). (d) As in (a) but for snow-water equivalent (mm).

almost doubles with soil layer (Fig. 9a). This is further examined in the next section.

6. Sources of water vapor in precipitation

Land surface conditions altered the amount of total precipitation on the global scale. The global mean of annual total precipitation is 996, 986, 1031, and 1024 mm for NMR, MR, MS, and MVS runs, respectively (Table 1). This includes the changes over ocean and land. Percentage of total precipitation that falls over land (open surface without permanent ice or snow cover occupies 25.6% of the total area) is 14.8%, 15.0%, 17.4%, and 21.7%, respectively, showing small increase with the presence of large-scale orography and large increase with vegetation. The total amount of annual evaporation from the land surface shows a similar result; respective percentages are 8.9%, 9.0%, 13.1%, and 16.2%. Comparison between MR, MS, and MVS shows a good agreement with the results of Milly and Dunne (1994) that annual land evaporation has a higher sensitivity to the water-holding capacity (their Fig. 12). This result illustrates an impact of land surface condition changes on global redistribution of water. This section examines the impacts on water vapor transport at different land areas in Eurasia and other continents.

Tracking of "tagged" water vapor was used to quantify the relative contributions of water vapor coming from different sources that precipitates in an arbitrary target region. The methodology that had been used in a previous version of the AGCM was used in this study (Numaguti 1999), which followed the similar tagging methods used in other previous studies (Koster et al.

TABLE 1. Area-averaged precipitation and evaporation for the globe, land (open-surface land, 25.6% in area), and ocean (71.4% in area). The percentage value to the global total is given in parentheses.

Total precipitation (mm)				
	NMR	MR	MS	MVS
Globe	996.	986.	1031.	1023.
Land	574. (14.8%)	578. (15.0%)	698. (17.4%)	867. (21.7%)
Ocean	1181. (84.6%)	1165. (84.4%)	1184. (82.0%)	1114. (77.7%)
Total evaporation (mm)				
	NMR	MR	MS	MVS
Globe	996.	986.	1031.	1023.
Land	346. (8.9%)	345. (9.0%)	527. (13.1%)	645. (16.2%)
Ocean	1268. (90.9%)	1255. (90.9%)	1252. (86.7%)	1200. (83.7%)

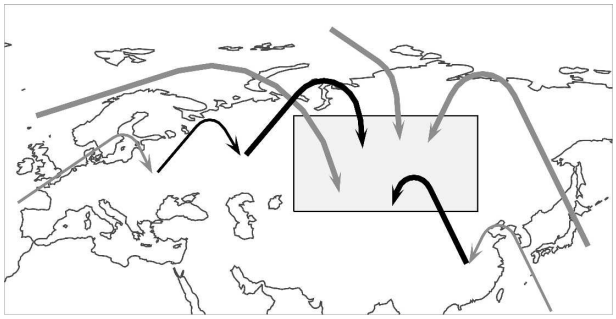

FIG. 10. Schematic presentation of water vapor tracing and water recycling.

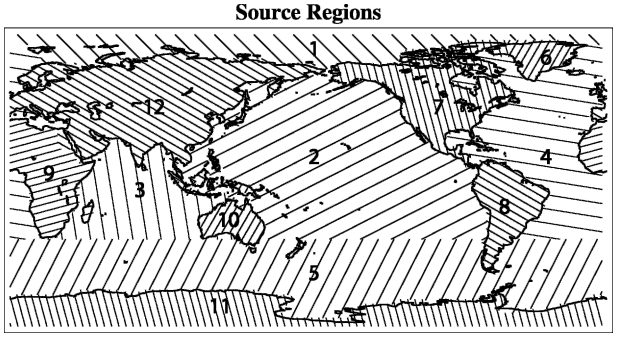

FIG. 11. Source regions for surface evaporation. There are five oceanic regions (1: Arctic, 2: Pacific, 3: Indian, 4: Atlantic, and 5: Southern) and seven land regions (6: Greenland, 7: North America, 8: South America, 9: Africa, 10: Oceania, 11: Antarctica, and 12: Eurasia).

1986, 1993; Bosilovich and Schubert 2002; Bosilovich et al. 2003). Figure 10 illustrates the motion of tagged vapor that ultimately precipitates in a target region in Eurasia. The evaporating water molecules are tagged with the "source" region, either from the land or ocean surface, and are subsequently advected following the calculated flow. Large-scale condensation and cumulus convection both form liquid water in an air parcel at each vertical level according to condensation conditions. It is assumed that the air is well mixed in the parcel so that the parcel contains water masses from different sources in proportion to the amount of vapor tagged with the "source" regions. Reevaporation is similarly considered. Water vapor that most recently evaporated from ocean surface (oceanic source) is shown in gray in the figure and vapor from land surface (land source) is shown in black. The globe is divided into five oceanic (Arctic, Pacific, Indian, Atlantic, and Southern) and seven continental (Greenland, North and South America, Africa, Oceania, Antarctica, and Eurasia) source regions as illustrated in Fig. 11. Relative contributions of the above 12 source regions in precipitation in a target region are computed by relative amounts of water vapor tagged with the sources (thick arrows in Fig. 11).

The primary impetus for tracing water vapor in continental precipitation was to investigate the relative impact of land surface conditions on the importance of ground surface to bring water inside continents. Recycling is a term used to refer to precipitation in which the vapor was evapotranspired at the same region (Brubaker et al. 1993; Eltahir and Bras 1996). Our interest is whether the precipitating water came directly from ocean surfaces or from land surfaces, and it is of little interest if it came from the same area. The term "recycling," or "continental recycling," in this study is therefore defined as precipitated water vapor that evaporated from a continental source region, regardless of definitions of geographical extent of target regions.

Model data spanning 10 yr after a 2-yr spinup period during which the model comes into equilibrium were used from all four simulations. The result of this version of the AGCM was substantially the same with the results of the previous version (Numaguti 1999). We also compared precipitation pattern and recycling ratio of our model's result with that of Brubaker et al. (1993) for their four regions, that is, western Eurasia, Mississippi, Amazon, and Sahel. The model reproduced the monthly precipitation in each region reasonably well, as compared with the result of Brubaker et al. and CMAP observation, except for known biases in Eurasia and Amazon (cf. Fig. 10 in Part I). Note that our respective source regions for the above four regions are Eurasia, North America, South America, and Africa, having much wider geographical extent than in Brubaker et al. Therefore, direct comparison of recycling ratio is difficult. The simulated annual mean recycling ratio is 12%, 44%, 44%, and 47% for western Eurasia, Mississippi, Amazon, and Sahel, respectively, while the corresponding values obtained by Brubaker et al. were 11%, 24%, 25%, and 35%. The reproduced seasonal cycle of recycling ratio is reasonable, although our estimate tends to be higher for the above reason (not shown).

a. Changes in sources of vapor in rainy season

Figure 12 shows the changes in the averaged relative contribution of major vapor sources in precipitation at the five target regions of our interest in or near Eurasia for the rainy season. The five regions are Maritime Continent (10°S–8°N, 90°–160°E), south and Southeast Asia (8°–25°N, 65°–110°E), east Asia (25°–45°N, 110°–145°E), Siberia (50°–80°N, 80°–140°E), and West Africa (0°–20°N, 20°W–10°E). The rainy season at these regions is defined in Table 2 in Part I.

In the Maritime Continent and the Tropics (Figs. 12a,b), the oceans remain the primary source of water

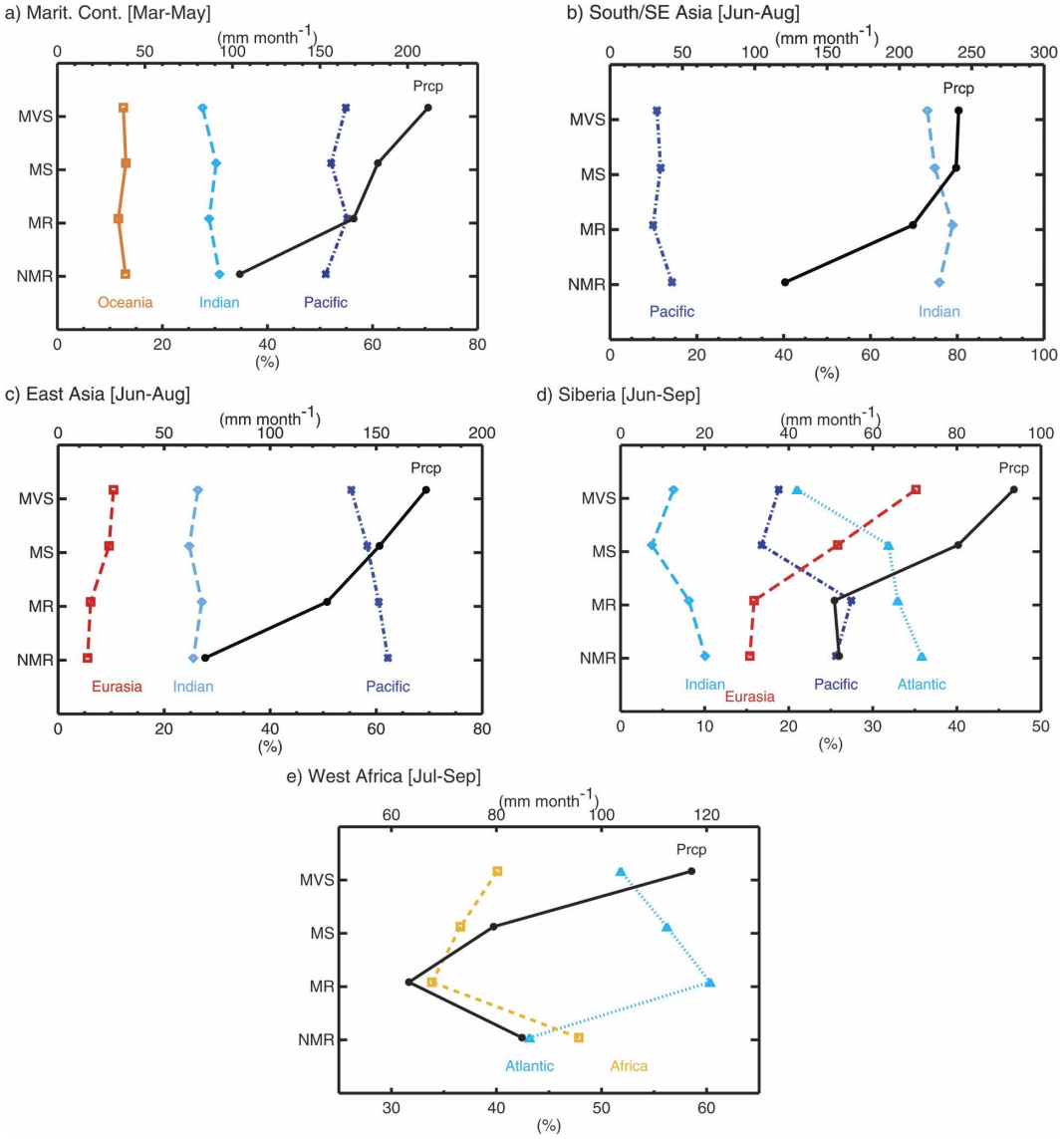

FIG. 12. (a) Averaged precipitation over the Maritime Continent (Indonesia) for March–May (closed circle), and the percentage of water vapor coming from different source regions. Lines with square (diamond, cross) symbols denote a source from Oceania (Indian, Pacific). Scale of the precipitation (percentage) is shown at top (bottom). (b) As in (a), but for south/Southeast Asia for June, July, and August. (c) As in (b), but for east Asia. Line with square symbols denotes Eurasian source. (d) As in (c), but for Siberia for June–September. Line with triangle symbols denotes the Atlantic source. (e) As in (d), but for West Africa for July, August, and September. Line with square symbols denotes African source.

vapor for precipitation, despite change in the amount of total precipitation. Contribution ratios are insensitive to land surface boundary changes because ocean-sourced convective rain dominates. In the extratropical continent, to the contrary, vegetation almost doubles total precipitation, with local (continental) source increasing more than twice (red line with square symbols in Fig. 12d) whereas the oceanic sources (Atlantic and Pacific) decrease by one-third. Large-scale topography has little influence on summer precipitation in Siberia. The results for the temperate eastern coastal area (Fig. 12c) are intermediate to the responses in tropical and high-latitude areas. The Pacific contribution is insensitive to the land surface changes. The contribution from the land (Eurasia) increases and that from the Indian Ocean decreases in east Asia as the mountains and vegetation are added.

The West Africa area shows a similar response to that of Siberia regarding precipitation amount and vapor source composition to vegetation in that the conti-

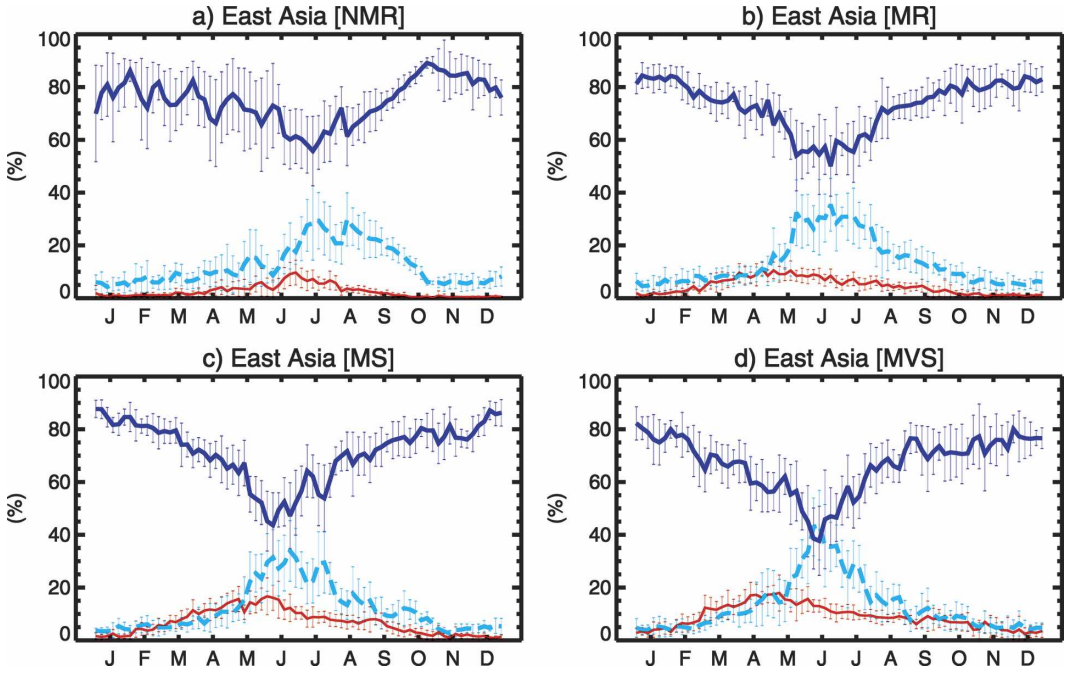

FIG. 13. Annual change of composition of water vapor from different source regions in precipitation over east Asia for (a) NMS, (b) MR, (c) MS, and (d) MVS. Solid (dashed, thin solid) line denotes percentage of water vapor coming from the Pacific (Indian, Eurasian) region.

nental contribution increases while the oceanic sources decrease. However, the Tibetan Plateau shows a different impact. Presence of the large-scale orography strengthens descent through changes in the Rossby wave pattern generated by the Tibetan orography and the increased diabetic heating (Rodwell and Hoskins 1996), to decrease total rainy-season precipitation by 60 mm in JJA, and the local vapor source by one-third.

b. East Asia

Figure 13 shows the impact of land surface conditions on the major sources of water vapor precipitates out in east Asia. The Pacific Ocean is the primary source throughout the year regardless of the surface conditions. The comparable contribution from other source regions is the Indian Ocean for the summer monsoon period. It increases as the mountains and vegetation are added. Continental contribution is not large for all the cases, although it increases in spring as the land surface conditions approach the present-day state.

c. Siberia

Summer is the season when recycled water vapor is the major vapor source for precipitation in Siberia (Brubaker et al. 1993; Numaguti 1999). Our result in Fig. 14 and in previous sections indicates vegetation is important in enhancing the continental recycling, with the vegetation skin and the soil layer having comparable impacts in our model. In winter, when biospheric activities are inactive, little impact is found from vegetation. Topography, in turn, shows a discernible impact during winter. The major vapor source remains the Atlantic Ocean, accounting for about 80% of the total water molecules in all the cases. The Indian source becomes comparable to the Pacific for the NMR run, although it becomes negligible when blocking mountains are present.

All the simulations with mountains (MR, MS, and MVS runs) show a large interannual variation in the winter transport. A circulation anomaly is associated with this interannual variation, showing a positive zonal wind anomaly between 30° and 50°N and a negative anomaly between 50° and 70°N when the Atlantic contribution is anomalously small. The interannual variability is not found for the NMR run, which implies a dynamical mechanism possibly involving orographically generated eddies and position or strength of the tropospheric jet stream. This issue is left to future investigations.

7. Discussions and summary

A series of simplistic simulations using an AGCM coupled to a simple land surface scheme quantitatively

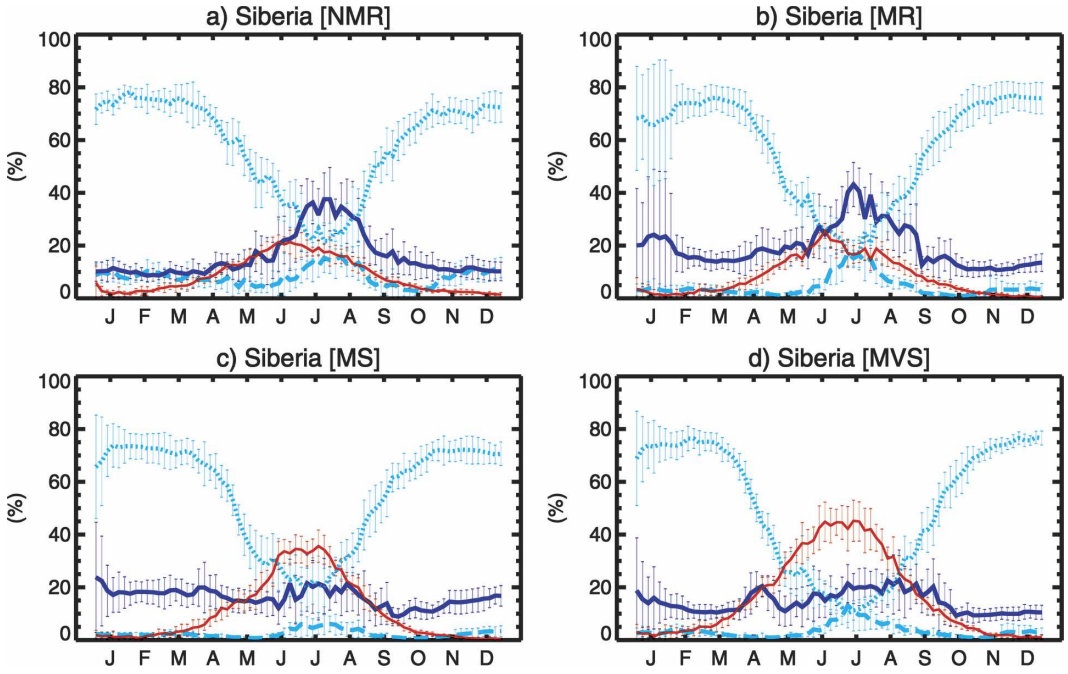

FIG. 14. As in Fig. 14, but over Siberia. Solid (dashed, dotted, thin solid) line denotes percentage of water vapor coming from the Pacific (Indian, Atlantic, Eurasian) region.

and qualitatively evaluated the relative impacts of basic factors in land surface conditions (i.e., large-scale orography, soil, and vegetation) on the hydroclimate of Eurasia. This study provides useful information regarding the basic land surface properties and their potential impacts that comprise basic parts of the present-day continental hydroclimate. It was decided to use a simple land surface scheme setting for this study because we attempted to draw a picture of the basic hydroclimate mechanisms related to the land surface conditions evaluated by the same configuration. A sophisticated scheme may obscure our intention by its complexity, which may interfere with the drastic setting, and the spread of the parameter space. However, it must be acknowledged that the result of the study may suffer from the insufficiency in the land hydrology scheme. Although our land surface scheme is improved from the original bucket-type hydrology scheme (Manabe et al. 1965) to include or consider some vital components of physiological–hydrological processes, simplistic treatment may still distort the water balance at surface as demonstrated in the Program for Intercomparison of Land Surface Parameterization Schemes (PILPS; Shao and Henderson-Sellers 1996) or other studies (e.g., Sato et al. 1989) for the standard bucket model. Therefore, the results of this study need be examined with caution in mind, and too-minute interpretation of absolute value comparisons may be inappropriate.

The model ocean in this study was prescribed from monthly climatological sea surface temperatures (SSTs) and sea ice concentrations. Recent studies have shown that changes in land surface conditions, such as orography, change the SST distribution through radiative and thermodynamic feedbacks between atmosphere and ocean (e.g., Kitoh 2002; Abe et al. 2004). For example, Abe et al. (2004) used a coupled atmosphere–ocean GCM to show that summer SST distributions in the Tropics are sensitive to a gradual decrease in surface elevation over the globe. As mountain heights decrease, SSTs in the west-to-central equatorial Pacific warm to 31°C. Several factors influence the increase, including suppressed upwelling due to weaker surface winds, an increase in solar radiation due to decreased cloud cover, and suppressed convection associated with the removal of orography. Other studies have suggested that the intensity of atmospheric response is weaker when it is forced by prescribed rather than interactive SSTs (e.g., Waliser et al. 1999; Fu and Wang 2004).

By using identical ocean boundary conditions in all model experiments, the fluctuations induced by oceanic variability are suppressed and the more subtle effects of land surface conditions can be evaluated. In addition, Abe et al. (2004) suggested that the influence of an interactive ocean is highest over the ocean and near the coasts. Continental interiors are more isolated. However, including an interactive ocean is an important fu-

ture research topic in this type of investigation as well as upgrading the biosphere–hydrology scheme in a continuous way. Another issue on improvement is subgrid-scale land hydrology (e.g., Gedney and Cox 2003). Inclusion of realistic runoff, and river and subsurface water discharge into the oceans is desired to close a hydrological cycle. More elaborate evaluations using output from a fully coupled atmosphere–ocean–land models will be necessary to evaluate more thoroughly the quantitative impacts of land surface changes.

Major results of Part II include the following. Land surface conditions had impacts on land precipitation on global scale; the global mean of annual total precipitation was 996, 986, and 1024 mm for NMR, MR, and MVS runs, respectively. A stronger impact was noticed on the percentage of precipitation that falls on land area (occupying 25.6% of the total surface). It was 14.8%, 15.0%, and 21.7%, and similarly, the percentage of land evaporation was 8.9%, 9.0%, and 16.2%, respectively. On the global and annual scale, vegetation showed a greater effect on the hydrological balance than the Asian mountains in our simulation. At regional and seasonal scales, however, large-scale orography and vegetation gave different impacts on the magnitude and distribution of energy and water cycle in different regions in different seasons. The summer hydroclimate in the Eurasian extratropical continent was sensitive to vegetation. In winter, mountains' impact overrode any atmospheric circulation changes.

Combined results from both parts of this study showed that the current hydroclimate of the earth has largely been shaped by an integrated system of land surface processes, within a range of properties of relatively long time scale, such as large-scale orography and vegetation. The presence of large-scale topography increased the atmospheric heating by the turbulent heat fluxes from the surface and strongly altered atmospheric circulation to transport more water and energy into the continental interior. Vegetation (soil and vegetation skin), although examined by a simple scheme, further increased the surface available energy and added small-scale features to the continental hydroclimate according to the vegetation type. It has recently been demonstrated that improved biosphere–land surface schemes, resolving subgrid-scale biophysical processes of shorter time scale, reproduce more realistic hydroclimatology (e.g., Xue et al. 2004). A fully coupled atmosphere–ocean–land–biosphere model of a finer horizontal resolution with a sophisticated physiology–hydrology scheme will enable further examinations of more minute impacts of vegetation and subsequently its changes on continental hydroclimate, for example, water availability and its change, following the large-scale land-use changes such as deforestation or forest fires. This will be an ingenuous extension of our investigation. In addition, an elaborate tracking of vapor transport has a potential to provide accurate information on the characteristics and sensitivity of vapor transport to those changes. Coupling of the vapor tracking with such a full model will derive information useful for water resource management in the future. These are the potential directions for future research.

Acknowledgments. The authors thank ISCCP and NASA Goddard Institute for Space Studies for providing climatology cloud data. The authors are grateful to three anonymous reviewers for their constructive comments that improved the original manuscript.

REFERENCES

Abe, M., A. Kitoh, and T. Yasunari, 2003: An evolution of the Asian summer monsoon associated with mountain uplift—Simulation with the MRI Atmosphere–Ocean Coupled GCM. *J. Meteor. Soc. Japan,* **81,** 909–933.

——, T. Yasunari, and A. Kitoh, 2004: Effects of large-scale orography on the coupled atmosphere–ocean system in the tropical Indian and Pacific Oceans in boreal summer. *J. Meteor. Soc. Japan,* **82,** 745–759.

Bosilovich, M. G., and S. D. Schubert, 2002: Water vapor tracers as diagnostics of the regional hydrologic cycle. *J. Hydrometeor.,* **3,** 149–165.

——, Y. C. Sud, S. D. Schubert, and G. K. Walker, 2003: Numerical simulation of the large-scale North American monsoon water sources. *J. Geophys. Res.,* **108,** 8614, doi:10.1029/2002JD003095.

Broccoli, A. J., and S. Manabe, 1992: The effects of orography on midlatitude Northern Hemisphere dry climates. *J. Climate,* **5,** 1181–1201.

Brubaker, K. L., D. Entekhabi, and P. S. Eagleson, 1993: Estimation of continental precipitation recycling. *J. Climate,* **6,** 1077–1089.

Buol, S. W., F. D. Hole, and R. J. McCracken, 1997: *Soil Genesis and Classification*. 4th ed. Iowa State University Press, 527 pp.

Charney, J. G., P. H. Stone, and W. J. Quirk, 1975: Drought in Sahara: A biogeophysical feedback mechanism. *Science,* **187,** 434–435.

——, W. J. Quirk, S. Chow, and J. Kornfield, 1977: A comparative study of the effects of albedo change on drought in semi-arid regions. *J. Atmos. Sci.,* **34,** 1366–1385.

Chen, G., 2004: A 10-yr climatology of oceanic water vapor derived from the TOPEX Microwave Radiometer. *J. Climate,* **17,** 2541–2557.

Delworth, T., and S. Manabe, 1988: The influence of potential evaporation on the variabilities of simulated soil wetness and climate. *J. Climate,* **1,** 523–547.

——, and ——, 1989: The influence of soil wetness on near-surface atmospheric variability. *J. Climate,* **2,** 1447–1462.

Dirmeyer, P. A., 1998: Land–sea geometry and its effect on monsoon circulation. *J. Geophys. Res.,* **103** (D10), 11 555–11 572.

——, and J. Shukla, 1996: The effect on regional and global cli-

mate of expansion of the world's deserts. *Quart. J. Roy. Meteor. Soc.,* **122,** 451–482.

Douville, H., F. Chauvin, and H. Broqua, 2001: Influence of soil moisture on the Asian and African monsoons. Part I: Mean monsoon and daily precipitation. *J. Climate,* **14,** 2381–2403.

Eltahir, E. A. B., and R. L. Bras, 1996: Precipitation recycling. *Rev. Geophys.,* **34,** 367–378.

Fu, X., and B. Wang, 2004: Differences of boreal summer intraseasonal oscillations simulated in an atmosphere–ocean coupled model and an atmosphere-only model. *J. Climate,* **17,** 1263–1271.

Gates, W. L., 1992: AMIP: The Atmospheric Model Intercomparison Project. *Bull. Amer. Meteor. Soc.,* **73,** 1962–1970.

Gedney, N., and P. M. Cox, 2003: The sensitivity of global climate model simulations to the representation of soil moisture heterogeneity. *J. Hydrometeor.,* **4,** 1265–1275.

Hahn, D. G., and S. Manabe, 1975: The role of mountains in the southern Asian monsoon circulation. *J. Atmos. Sci.,* **32,** 1515–1541.

He, H., J. W. McGinnis, Z. Song, and M. Yanai, 1987: Onset of the Asian summer monsoon in 1979 and the effect of the Tibetan Plateau. *Mon. Wea. Rev.,* **115,** 1966–1995.

Henderson-Sellers, A., P. Irannejad, K. McGuffie, and A. J. Pitman, 2003: Predicting land-surface climates—Better skill or moving targets? *Geophys. Res. Lett.,* **30,** 1777, doi:10.1029/2003GL017387.

Jenny, H., 1941: *Factors of Soil Formation; A System of Quantitative Pedology*. Dover Publications, 281 pp.

Kitoh, A., 2002: Effect of large-scale mountains on surface climate—A coupled ocean–atmosphere general circulation. *J. Meteor. Soc. Japan,* **80,** 1165–1181.

Koster, R., J. Jouzel, R. Suozzo, G. Russell, W. Broecker, D. Rind, and P. Eagleson, 1986: Global sources of local precipitation as determined by the NASA/GISS GCM. *Geophys. Res. Lett.,* **13,** 121–124.

——, D. Perry de Valpine, and J. Jouzel, 1993: Continental water recycling and H218O concentrations. *Geophys. Res. Lett.,* **20,** 2215–2218.

Kutzbach, J. E., W. L. Prell, and W. F. Ruddiman, 1993: Sensitivity of Eurasian climate to surface uplift of the Tibetan Plateau. *J. Geol.,* **101,** 177–190.

Luo, L., and Coauthors, 2003: Effects of frozen soil on soil temperature, spring infiltration, and runoff: Results from PILPS 2(d) Experiment at Valdai, Russia. *J. Hydrometeor.,* **4,** 334–351.

Manabe, S., J. Smagorinsky, and R. F. Strickler, 1965: Simulated climatology of a general circulation model with a hydrologic cycle. *Mon. Wea. Rev.,* **93,** 769–798.

Milly, P. C. D., and K. A. Dunne, 1994: Sensitivity of the global water cycle to the water-holding capacity of land. *J. Climate,* **7,** 506–526.

Mitchell, T. D., and P. D. Jones, 2005: An improved method of constructing a database of monthly climate observations and associated high-resolution grids. *Int. J. Climatol.,* **25,** 693–712

Numaguti, A., 1999: Origin and recycling processes of precipitating water over the Eurasian continent: Experiments using an atmospheric general circulation model. *J. Geophys. Res.,* **104** (D2), 1957–1972.

Rodwell, M., and B. Hoskins, 1996: Monsoons and the dynamics of deserts. *Quart. J. Roy. Meteor. Soc.,* **122,** 1385–1404.

Sato, N., P. J. Sellers, D. A. Randall, E. K. Schneider, J. Shukla, J. L. Kinter III, Y.-T. Hou, and E. Albertazzi, 1989: Implementing the Simple Biosphere model in a general circulation model. *J. Atmos. Sci.,* **46,** 2757–2782.

Shao, Y., and A. Henderson-Sellers, 1996: Modeling soil moisture: A project for intercomparison of land surface parameterization schemes phase 2(b). *J. Geophys. Res.,* **101** (D3), 7227–7250.

Shukla, J., and Y. Mintz, 1982: Influence of land-surface evapotranspiration on the Earth's climate. *Science,* **215,** 1498–1501.

Viterbo, P., A. Beljaars, J.-F. Mahfouf, and J. Teixeira, 1999: The representation of soil moisture freezing and its impact on the stable boundary layer. *Quart. J. Roy. Meteor. Soc.,* **125,** 2401–2426.

Waliser, D. E., K. M. Lau, and J. H. Kim, 1999: The influence of coupled sea surface temperatures on the Madden–Julian oscillation: A model perturbation experiment. *J. Atmos. Sci.,* **56,** 333–358.

Xie, P., and P. A. Arkin, 1997: Global precipitation: A 17-year monthly analysis based on gauge observation, satellite estimates, and numerical model outputs. *Bull. Amer. Meteor. Soc.,* **78,** 2539–2558.

Xue, Y., H.-M. H. Juang, W.-P. Li, S. Prince, R. DeFries, Y. Jiao, and R. Vasic, 2004: Role of land surface processes in monsoon development: East Asia and West Africa. *J. Geophys. Res.,* **109,** D03105, doi:10.1029/2003JD003556.

Yanai, M., and C. Li, 1994: Mechanism of heating and the boundary layer over the Tibetan Plateau. *Mon. Wea. Rev.,* **122,** 305–323.

——, ——, and Z. Song, 1992: Seasonal heating of the Tibetan Plateau and its effects on the evolution of the Asian summer monsoon. *J. Meteor. Soc. Japan,* **70,** 319–351.

Yasunari, T., K. Saito, and K. Takata, 2006: Relative roles of large-scale orography and land surface processes in the global hydroclimate. Part I: Impacts on monsoon systems and the Tropics. *J. Hydrometeor.,* **7,** 626–641.